Different crystal morphologies lead to slightly different conformations of light-harvesting complex II as monitored by variations of the intrinsic fluorescence lifetime

van Oort, B.F.; Marechal, A; Ruban, A.V.; Robert, B.; Pascal, A.A.; de Ruijter, N.C.A.; van Grondelle, R.; van Amerongen, H.

published in
Physical Chemistry Chemical Physics - PCCP
2011

DOI (link to publisher)
10.1039/c1cp20331b

document version
Publisher's PDF, also known as Version of record

PCCP

View Online
Dynamic Article Links

Cite this: *Phys. Chem. Chem. Phys.*, 2011, **13**, 12614–12622

www.rsc.org/pccp

PAPER

Different crystal morphologies lead to slightly different conformations of light-harvesting complex II as monitored by variations of the intrinsic fluorescence lifetime†

Bart van Oort,*[ab] Amandine Maréchal,[c] Alexander V. Ruban,[d] Bruno Robert,[c] Andrew A. Pascal,[c] Norbert C. A. de Ruijter,[e] Rienk van Grondelle[a] and Herbert van Amerongen[bf]

Received 8th February 2011, Accepted 17th May 2011
DOI: 10.1039/c1cp20331b

In 2005, it was found that the fluorescence of crystals of the major light-harvesting complex LHCII of green plants is significantly quenched when compared to the fluorescence of isolated LHCII (A. A. Pascal *et al.*, *Nature*, 2005, **436**, 134–137). The Raman spectrum of crystallized LHCII was also found to be different from that of isolated LHCII but very similar to that of aggregated LHCII, which has often been considered a good model system for studying nonphotochemical quenching (NPQ), the major protection mechanism of plants against photodamage in high light. It was proposed that in the crystal LHCII adopts a similar (quenching) conformation as during NPQ and indeed similar changes in the Raman spectrum were observed during NPQ *in vivo* (A. V. Ruban *et al.*, *Nature*, 2007, **450**, 575–579). We now compared the fluorescence of various types of crystals, differing in morphology and age. Each type gave rise to its own characteristic mono-exponential fluorescence lifetime, which was 5 to 10 times shorter than that of isolated LHCII. This indicates that fluorescence is not quenched by random impurities and packing defects (as proposed recently by T. Barros *et al.*, *EMBO Journal*, 2009, **28**, 298–306), but that LHCII adopts a particular structure in each crystal type, that leads to fluorescence quenching. Most interestingly, the extent of quenching appears to depend on the crystal morphology, indicating that also the crystal structure depends on this crystal morphology but at the moment no data are available to correlate the crystals' structural changes to changes in fluorescence lifetime.

Introduction

A crucial step in the biological use of solar energy is the photosynthetic conversion of the photonic energy into chemical energy. In oxygenic photosynthetic organisms two protein supercomplexes, named photosystems I and II (PSI, PSII), work in tandem to facilitate the production of ATP and NADPH. These supercomplexes are highly organized: their reaction centers, responsible for charge separation, are surrounded by light-harvesting complexes (LHCs). The LHCs bind large numbers of photochemically-inactive pigments, which absorb and efficiently transfer light energy, thus greatly enhancing the effective absorption cross-section of the system.[1–3] This is highly beneficial for plants growing at low-light intensity, but may lead to photodamage under high-light conditions. Light intensity can fluctuate greatly during the course of the day (and even within seconds in some cases), and many photosynthetic organisms have developed protective mechanisms which guard against photoinduced damage.

Non-photochemical quenching (NPQ) is one of these photoprotection mechanisms.[4] NPQ consists of several components, the most important one being the rapidly reversible qE (for recent reviews see ref. 5–7). qE is triggered by a ΔpH across the photosynthetic membrane, and it is dynamically controlled by the regulatory PsbS protein and by the xanthophyll-cycle

[a] *VU University Amsterdam, Faculty of Sciences, Department of Physics and Astronomy, De Boelelaan 1081, 1081 HV Amsterdam, The Netherlands. E-mail: b.f.van.oort@vu.nl; Fax: +31 (0)20 598 7999; Tel: +31 (0)20 598 6383*
[b] *Wageningen University, Laboratory of Biophysics, PO Box 8128, 6700 ET, Wageningen, The Netherlands*
[c] *Commisariat à l'Energie Atomique (CEA), Institut de Biologie et Technologies de Saclay (iBiTecS), URA 2096, Gif sur Yvette, F-91191, France*
[d] *School of Biological and Chemical Sciences, Queen Mary University of London, Mile End Road, London, E1 4NS, UK*
[e] *Wageningen University, Laboratory of Plant Cell Biology, PO Box 633, 6700 AP Wageningen, The Netherlands*
[f] *MicroSpectroscopy Centre, Wageningen University, PO Box 8128, 6700 ET, Wageningen, The Netherlands*
† Electronic supplementary information (ESI) available: Raman spectra, and spectral fitting and 3D reconstruction of SPIM data. See DOI: 10.1039/c1cp20331b

carotenoids (violaxanthin, antheraxanthin and zeaxanthin).[7–9] qE leads to the dissipation of absorbed energy as heat, thereby acting as a safety valve to reduce the excitation pressure in PSII.[4] It thereby leads to quenching of chlorophyll (Chl) fluorescence. This offers the possibility to study qE with the use of fluorescence (quenching), a method that is being used extensively.

Despite intense recent research, there is still strong debate about the precise mechanism(s) and location(s) of qE. Most researchers agree that qE occurs in the LHC complexes, although it is not clear whether this is in the major LHC (LHCII) (as initially proposed in ref. 10), and/or (one or more of) the minor LHCs.[11–15] Several quenching mechanisms have been proposed, *e.g.* quenching by a Chl–Chl charge transfer (CT) state,[11,16] by formation of a xanthophyll cation radical,[13,17] by increased coupling of a Chl with a short-lived xanthophyll excited state,[18–20] by a Chl–Chl dimer/excimer,[21] and by energy transfer to a lutein.[22]

Irrespective of the quenching mechanism, a "change" has to occur in order to create the quenching species (the quencher). This change can be attachment/detachment of an external quencher to the LHCs, or a change within LHCs (which could be mediated by attachment/detachment of an allosteric moderator, such as PsbS). Quenching can be induced without changing pigment composition,[22] therefore the only way to produce/stabilize quenchers is by modification of the distances and/or relative orientations between pigments and/or between pigments and the protein. In other words, a structural change must occur. This structural change was termed a "conformational change" (or conformational switch),[10] and its nature has been heavily debated.[11,13,16,17,20,23–25]

Theoretical studies suggest that very minor structural changes can induce dramatic spectral changes in LHCII.[26] Indeed, LHCII complexes with different extents of quenching are known to exist with only very small volume differences (0.006%V).[27] This makes the conformational changes hard to observe in protein-structure studies. Therefore, conformational changes have been studied in an indirect way, by their effect on pigments and pigment–pigment interactions, both *in vitro* and *in vivo*. Several *in vitro* assays with LHCs (*e.g.* aggregation,[28] detergent removal without aggregation[29] and integration into liposomes[30]) showed fluorescence quenching, accompanied by spectroscopic signatures similar to those observed during quenching *in vivo* (*e.g.* ref. 11, 22, and 31). The spectroscopic signatures point at twisting of the neoxanthin molecule.[22,25] As mutants lacking neoxanthin are not affected in NPQ,[32] this twisting of neoxanthin is probably not directly related to the quencher but is rather a reflection of the conformational changes that lead to quencher formation.

The publication of the 2.7 Å resolution crystal structures of LHCII from spinach[33] and pea[34] gave better insight into the pigment organization in this protein. Interestingly, the chlorophyll fluorescence of the spinach LHCII crystals appeared to be strongly quenched relative to that of solubilized LHCII trimers.[25] Moreover, the Raman and 77 K fluorescence spectra of the crystals showed characteristics of LHCII *in vitro* assays for qE (neoxanthin twist; fluorescence red shift and broadening). These results led to the suggestion that a quenched conformation/structure had been crystallized.[25]

This interpretation was recently challenged by Barros *et al.*, based on low-temperature fluorescence emission spectra and decay kinetics obtained on pea LHCII crystals.[24] Barros *et al.* showed that reabsorption effects in these optically dense crystals can lead to a similar red shift of the fluorescence as reported in ref. 25. Furthermore, they observed substantial heterogeneity in the fluorescence lifetimes and claimed that the amount of fluorescence quenching was small when compared to the fluorescence of trimeric LHCII in solution. In aggregates, which were more strongly quenched than the crystals, they also found strong heterogeneity, and ascribed the quenching to the random presence of fluorescence quenchers. This led the authors to suggest that the fluorescence quenching in crystals is not a property of each LHCII trimer in the crystal, but is due to crystal imperfections (impurities or irregularities at domain boundaries) that act as quenchers for many coupled LHCII trimers in the crystal lattice.

Further objections against the occurrence of conformational changes came from the crystallographic B-factors and the strong structural resemblance of LHCII in the two different crystal morphologies (from spinach[33] and pea[34]), grown in very different conditions. However, both objections have recently been challenged both on theoretical[26] and experimental grounds (the volume difference between quenched/unquenched LHCII can be too small to be detected at 2.7 Å resolution).[27]

Summarizing, two mechanisms have been proposed to explain the quenching of chlorophyll fluorescence in LHCII crystals: (1) each trimeric complex in the crystal is in a quenched state ("intratrimeric quenching");[25] and (2) various impurities/crystal defects are randomly distributed in the crystal (like in LHCII aggregates), and quench the fluorescence of many LHCII trimers in their vicinity ("random quenching").[24] For proper interpretation of the observed quenching, and to correlate this with the concomitant spectroscopic differences as compared to unquenched LHCII, it is important to distinguish between these two mechanisms.

We try to solve this issue in the present study by measuring room temperature spatially- and time-resolved fluorescence of crystals of different morphologies and age. Random quenchers are expected to have varying spectral properties, quenching strengths and concentrations (within and between crystals) and are expected to lead to a large variation of fluorescence lifetimes within and between crystals. Therefore, we compared different crystals and tested the degree of multi-exponentiality of the fluorescence decay curves of single crystals.

All crystals appear to be strongly quenched as compared to solubilized LHCII trimers. The fluorescence kinetics, however, are very homogeneous throughout the crystal, and they are essentially mono-exponential. Different crystal morphologies show different fluorescence lifetimes, even when grown in the same drop, whereas similar crystal morphologies also show similar lifetimes. These observations and their comparison with previous work[24,25] support the model in which quenching of LHCII crystals is ascribed to a conformational change within each trimer (relative to unquenched LHCII), rather than the model of randomly-present quenchers.

Materials and methods

LHCII crystal preparation

LHCII from spinach (*Spinacia oleracea*) was isolated, purified and crystallized as described in ref. 33.

Steady-state fluorescence of LHCII trimers and aggregates

Solubilized trimeric LHCII from spinach (*Spinacia oleracea*) was prepared either as described previously,[35] followed by suspending in a 20 mM HEPES buffer (pH 7.6) with 0.03% (0.6 mM) β-dodecylmaltoside (β-DM), or by solubilizing LHCII crystals directly into this buffer. Aggregates were prepared by diluting trimeric LHCII into a detergent-free buffer. Thus, the β-DM concentration was lowered to 0.0003% (0.6 μM), *i.e.* far below the critical micelle concentration (~0.15 mM).[36] Fluorescence emission spectra were measured at room temperature, with an optical density of 0.05 cm^{-1} at 675 nm, using excitation at 430 nm, on a Spex-Fluorolog 3.2.2 spectrofluorimeter (HORIBA Jobin-Yvon, Edison, NJ).

Fluorescence lifetime imaging microscopy

Time-resolved fluorescence of LHCII crystals was measured by fluorescence lifetime imaging microscopy (FLIM) with the setup described previously. Two-photon excitation was achieved by focusing laser pulses (wavelength 860 nm, pulse duration 150 fs, repetition rate 76 MHz) into the sample with a 60× water-immersion objective lens (CFI Plan Apochromat, numerical aperture 1.2, Nikon, Tokyo, Japan). Fluorescence was separated from excitation light with a dichroic mirror (FF 495-DiO2, Semrock, NY). A second dichroic mirror (770DCXR, Chroma Technology Corp., McHenry, IL) directed the fluorescence to a Hamamatsu R3809U MCP PMT detector (Hamamatsu City, Japan) for non-descanned single-photon counting detection. In front of the detector were either two bandpass filters of 700 nm (75 nm width, HQ700/75 Chroma Technology Corp.), or one bandpass filter of 730 nm (45 nm width, XF1097 730AF45, Omega Optical, Brattleboro, VT). Image dimensions were either (i) 256 × 256 pixels (0.5 μm per pixel) with decay traces of 64 time channels of 200 ps, or (ii) 64 × 64 pixels with decay traces of 1024 time channels of 12.2 ps. In the latter case, pixel step sizes ranged from 0.5 to 2.0 μm per pixel. For technical reasons it is impossible to work with higher numbers of time channels in combination with a large number of pixels (and a concomitantly larger field of view). The fluorescence intensity scaled quadratically with laser power, as expected for two-photon excitation, and the fluorescence kinetics did not depend on excitation power, as expected for annihilation-free experiments (results not shown). The lateral spatial resolution of the microscope was determined from an image of ten fluorescent beads (200 nm diameter, dark red, excitation/emission = 660/680 nm, FluoSpheres, Invitrogen) stuck to a cover slip. The resolution (defined as the full width at half maximum (FWHM) of the point spread function (psf)) was corrected for the bead size by deconvolution, and was determined to be 361 ± 11 nm. The vertical resolution was determined in the same way, and was approximately 1 μm. Thus, the excited volume was approximately 0.1 fl. This volume of the crystal contains on the order of 10^5 LHCII trimers.

The fluorescence decay curves were analyzed by the SPCImage software package (Becker & Hickl), including binning over 3 × 3 pixels and convolution with the instrument response function (measured from the 6-ps-decay of pinacyanol iodide in methanol).[37] The amplitude-weighted average fluorescence lifetime ($\langle\tau\rangle$) was calculated from the amplitudes (p_i) and lifetimes (τ_i), according to $\langle\tau\rangle = \sum_{i=1}^{N} p_i\tau_i \Big/ \sum_{i=1}^{N} p_i$. Analyses without pixel binning gave essentially the same results, but with greater fitting uncertainty due to the lower signal-to-noise ratio.

Spectral imaging

A spectral image requires the creation of a 4D data set that contains a collection of 3D images of the same viewfield captured at different spectral bands. Spectral imaging microscopy (SPIM) provides a complete spectrum of the specimen at every pixel location $I(x,y,z,\lambda)$, called λ-stack. In this study we used the LSM 510-META18 (Carl Zeiss, Jena, Germany) and three lasers for excitation: 488 nm Ar laser, 543 nm and 633 nm HeNe laser. Images were acquired with a 63× oil immersion objective NA 1.4. The same main dichroic mirror 405/488/543/633 was used for all excitations. With a diffraction grating the emitted fluorescence is directed on an array of bandwidth channels in the META multi-anode photomultiplier. Emission profiles were obtained from λ-stacks in the range of 646–753 nm in a series of 10 PMTs of the META channel each collecting photons with a 10.7 nm bandwidth. Z stacks were obtained with 1 airy unit, corresponding to optical slices of 0.9–1.0 μm, with each 3D pixel (voxel) representing 0.28 × 0.28 × 2.0 μm in xyz (the lateral spatial resolution, defined as the full width at half maximum of the point spread function, was 280 nm). By analysing λz-stacks a shift in the emission maxima can be related to the distance from the crystal surface.

Resonance Raman spectroscopy

77 K Resonance Raman spectra were recorded using the set-up described previously,[38] for single LHCII crystals frozen on a glass plate in mother liquor.[33]

Results

SPIM

One of the problems of measuring time-resolved fluorescence of optically dense LHCII crystals is reabsorption. Therefore we applied spectrally-resolved microscopy (SPIM) of the same crystals that were used for time-resolved microscopy. In each 3-dimensional pixel (voxel) of a crystal a fluorescence emission spectrum was recorded. The effect of reabsorption is paramount in the emission spectra of regions beyond the crystal surface (Fig. 1). At 5 μm into the crystal, the spectrum has shifted by more than 10 nm. From 0 to ~3 μm the spectrum does not change, but the intensity increases. This is due to the size of the excitation/detection spot; at 0 μm this spot only partly overlaps with the crystal.

The absolute detected fluorescence intensity decreases at increasing distance to the crystal surface. The extent of loss is

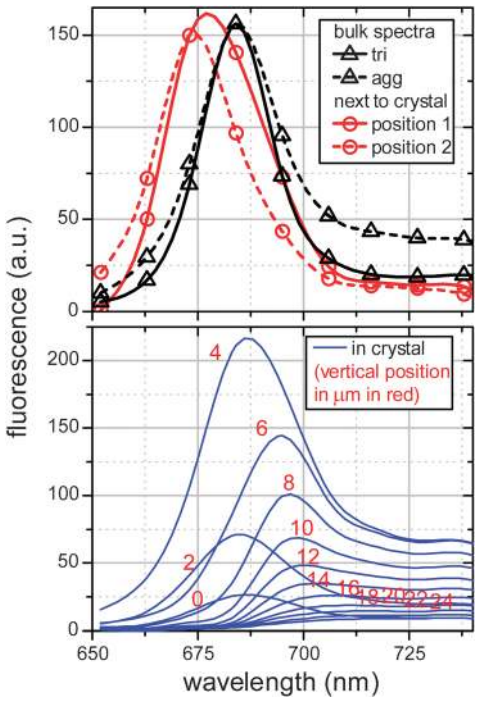

Fig. 1 Emission spectra of a single five-week-old LHCII crystal, recorded by SPIM, at different depths relative to the surface of the crystal (lower image, depth indicated in red). The upper image shows emission spectra at two positions in the fluid surrounding the crystal ("position 1" and "position 2") and spectra of trimeric ("tri") and aggregated LHCII ("agg") in solution. Excitation was at 543 nm. The fluorescence was recorded in each 3-dimensional voxel of a crystal and its surrounding fluid. See ESI† for results of spatially resolved analysis and for mathematical modelling of the effect of reabsorption on spectral shape and intensity.

due to both absorption of the excitation light, and reabsorption of the emitted light. Both effects lead to an exponential decay of fluorescence intensity as a function of depth in the crystal. In addition, reabsorption leads to a red-shift of the detected signal. It is also possible that the spectrum and/or quantum yield of LHCII varies throughout the vertical position in the crystal, which may also account for the observed spectral changes in Fig. 1. The effects of absorption and reabsorption were analyzed using the absorption and emission spectra of trimeric LHCII in detergent solution. This could quantitatively explain the observed fluorescence intensity and spectra as a function of vertical position for three different excitation wavelengths (488, 543, 633 nm, see ESI†). The conclusion must be that the intrinsic molecular fluorescence emission spectrum and quantum yield do not depend on the vertical position in the crystal (at the current spatial and spectral resolution).

At room temperature the differences between emission spectra of trimeric and aggregated LHCII are less pronounced than at cryogenic temperatures.[28] The spectrum of aggregates is slightly red-shifted and broadened relative to that of trimers[28] (see also Fig. 1). The emission spectrum of the outer layers of the crystal, which are least distorted by reabsorption, is more similar to that of LHCII aggregates than to that of trimers (Fig. 1, upper image and lower image traces 0, 2, and 4). Spectra recorded in regions next to the crystals are blue-shifted (*e.g.* red lines in Fig. 1), and are probably due to unfolded LHCII or free pigments. With the results in Fig. 1 in mind, we took great care to excite the crystals at their surface during the fluorescence lifetime imaging (FLIM) experiments (although it should be noted that fluorescence decay kinetics are not affected by reabsorption, provided all emitters are spectrally identical).[39]

FLIM

FLIM experiments were performed either with a large field of view and intermediate time resolution, or with a smaller field of view, and high time resolution. The first type of experiment is valuable to get an overview of the different crystals present in the samples (Fig. 2). The second type was used for detailed analysis of individual crystals (Fig. 3). The color coding for the lifetimes in Fig. 2 shows very clearly that different crystal morphologies correspond to different average lifetimes, and moreover that these lifetimes are very homogeneous over the crystals. The large crystals have average fluorescence lifetimes of 500–550 ps, while the smaller, rod-shaped ones are at 400–450 ps.

The centers of the bigger crystals show slightly shorter fluorescence lifetimes than the edges. This is probably due to lower count rates in the center, which leads to lower numbers of photons in the tails of the decay curves. At these low numbers the Poissonian noise distribution can no longer be

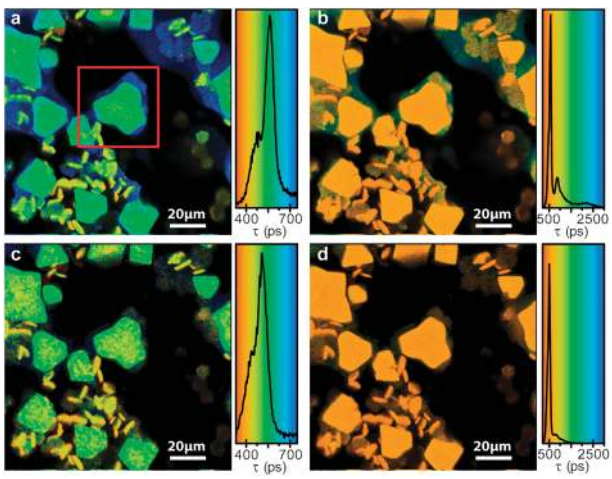

Fig. 2 False-colour fluorescence lifetime images of a drop containing three-weeks-old LHCII crystals. The colour codes for the fluorescence lifetime, as shown in the background of the histograms. The histograms show the number of pixels with a given fluorescence lifetime. The colour scale of the left images ranges from 330 ps (red) to 750 ps (blue). For the right images this is 200–3000 ps. Four discrete morphologies of LHCII crystals are visible: rod-shaped crystals (~400–450 ps; yellow in the left images), big crystals (500–550 ps; green on the left, orange on the right), LHCII with lifetime 800–1000 ps (near the edges of the crystals; dark blue on the left, yellow on the right) and LHCII with lifetime 2–3 ns (further away from the crystals; dark blue in both images). Experimental details: 256 × 256 pixels, 0.5 μm per pixel, 64 time channels of 200 ps in each pixel. Two-photon excitation was at 860 nm, detection at 670–730 nm (upper images) or at 710–750 nm (lower images). The red box indicates the region studied at higher temporal resolution in Fig. 3 and 4.

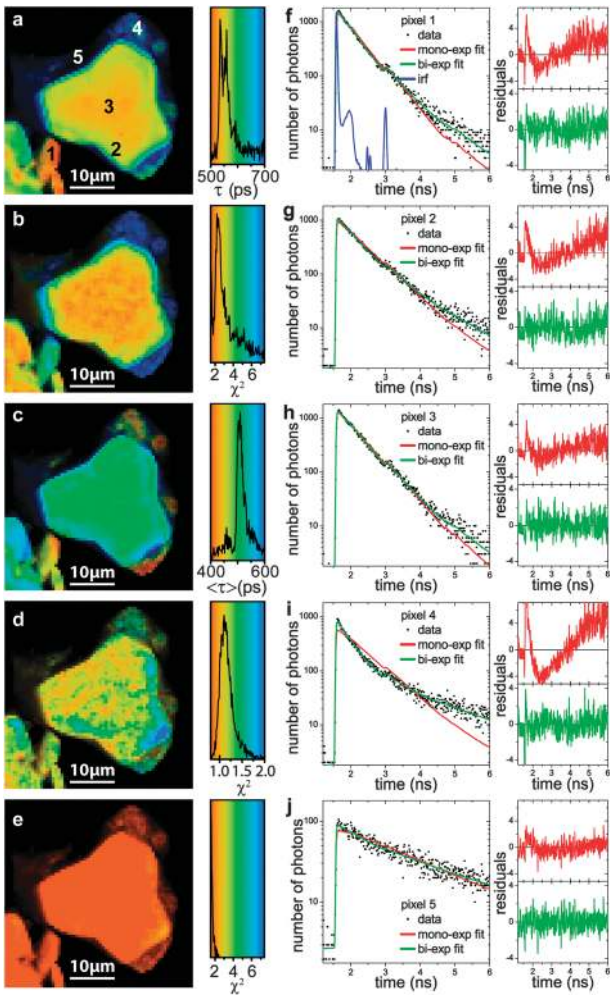

Fig. 3 Fitting results of FLIM data, with mono- and bi-exponential fits. False-colour image coding for the mono-exponential decay lifetime (a) and χ^2 of that fit (b), average lifetime from the bi-exponential decay ((c), calculated from the fluorescence lifetimes and relative amplitudes in Fig. 4) and χ^2 of that fit ((d, e); (e) on the same colour scale as (b)). The histograms next to each image show the number of pixels with certain values, and the backgrounds of the histograms give the colour code of the corresponding image. Decay traces from 5 different pixels (1–5 in A, 3 × 3 pixel binning) are shown in (f)–(j), with the fitted curves (red mono, green bi-exponential) and plots of the residuals and the autocorrelation thereof. Experimental details: 64 × 64 pixels, 0.5 μm per pixel, 1024 time channels of 200 ps in each pixel. Two-photon excitation was at 860 nm, detection at 670–730 nm.

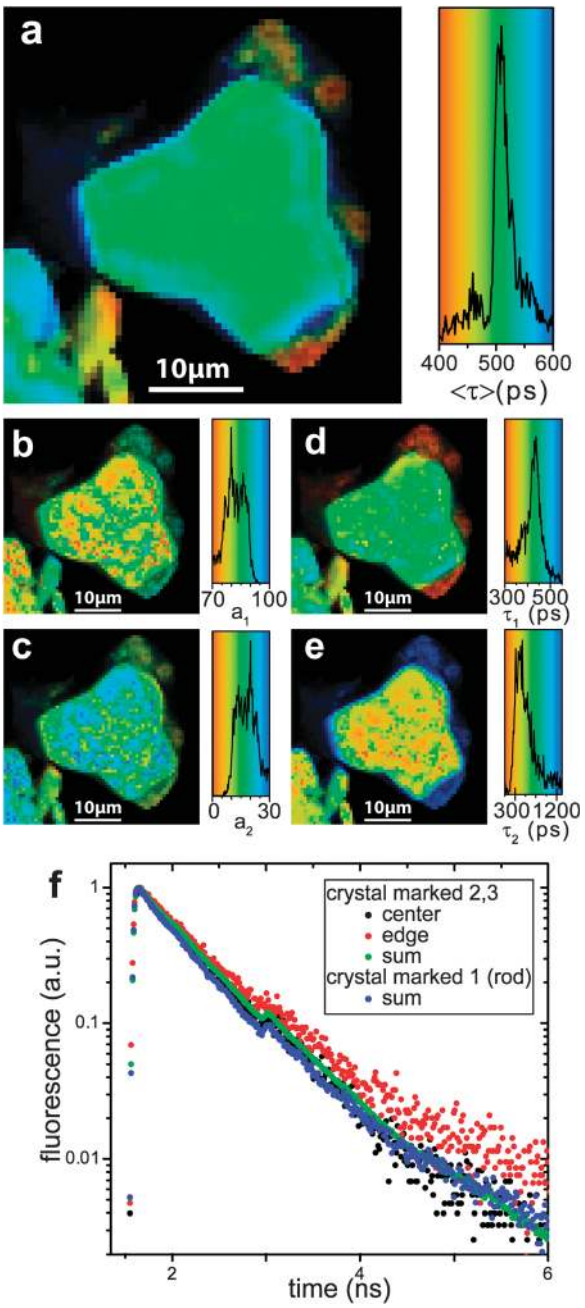

Fig. 4 Fitting results of FLIM data with a mono- or bi-exponential decay. False-colour images of average fluorescence lifetime (a), relative amplitudes $a_i = p_i \Big/ \sum_{i=1}^{N} p_i$ (b, c) and lifetimes (d, e) detected at 670–730 nm. Decay curves of the crystal marked 1 and 2, 3 in Fig. 3A (average of the edges or the centre of the crystal, and of the total crystals). Experimental details: 64 × 64 pixels, 0.5 μm per pixel, 1024 time channels of 12.2 ps in each pixel. Two-photon excitation was at 680 nm, detection at 670–730 nm.

approximated as Gaussian, and the fitting software yields slightly less reliable results (a slight overestimation of the lifetimes).[40] Additionally, it is more difficult to reliably subtract the dark counts (0–5 counts per channel at 3 × 3 pixel binning) at low photon numbers, leading to small but systematic deviations.

At longer wavelengths (710–750 nm), the fluorescence decay seems to be slightly faster (~30 ps) than at shorter wavelengths (670–730 nm). However, it is not clear whether this effect is real, because (i) the number of photons is lower at longer wavelengths and (ii) the fluorescence of the reference compound (pinacyanol iodide in methanol) is very weak at the longer wavelengths, and consequently the instrument response can be less accurately determined than at shorter wavelengths. In the regions surrounding the crystals the fluorescence decays much slower, with lifetimes of either 800–1000 ps or 2–3 ns.

The spatial region marked by the red box in Fig. 2a was studied in more detail with high temporal resolution (1024 channels/12.5 ns instead of 64 channels/12.5 ns). The results (Fig. 3a) compare well with those from intermediate

temporal resolution, except for a small underestimation of the lifetimes in the latter case (Fig. 2). The data were fitted with either a mono-exponential or a bi-exponential decay. The bi-exponential fit was slightly better than the mono-exponential one (as judged from the χ^2 values, Fig. 3b, d and e). This is confirmed by the decay traces, fits and fit residuals of different regions of the image (Fig. 3f–h). All the fit results of this image are shown in Fig. 4, and summarized in Table 1.

The decay is nearly mono-exponential, with ~15% of an ~0.8 ns decay component, and a major decay component of ~0.4 ns. The amplitude-weighted average fluorescence lifetimes are ~550 ps (big crystal), ~520 ps (rods), ~750 ps (next to big crystal, near to point 4) and 2–2.5 ns (near to point 5).

The sum fluorescence decay of the entire crystal, however, is virtually mono-exponential (Fig. 4). Apparently the bi-exponentiality is (mainly) due to baseline effects/uncertainties due to the low count rate in the tail of the decay curve. Therefore in the following we shall focus on the average fluorescence lifetime. The same group of crystals was also studied with detection from 710 to 750 nm, and the results were similar to those with detection between 670 and 730 nm (Fig. 4 and Table 1). The fluorescence lifetimes at 710 to 750 nm are consistently slightly shorter than at 670–730 nm. This is (at least partly) due to a small impurity <1% in the reference compound used to measure the instrumental response function. This impurity decays in a few hundreds of picoseconds. It is only present with red detection, where the reference compound fluoresces only weakly. The distortion yields a small underestimation of the fluorescence lifetimes.

There are no large variations of the fluorescence lifetime within the big crystal shown in Fig. 2–4. The small, rod-shaped crystals however (near pixel 1 in Fig. 2–4) consistently show faster fluorescence decay curves than the big crystal, measured at both intermediate and high temporal resolution. This points to a systematic relationship between crystal type and fluorescence lifetimes. We further investigated this by recording the fluorescence of several tens of crystals. Different crystal morphologies were observed: (i) several sizes of hexagonal crystals (15–125 μm), (ii) small rod-shaped and (iii) large distorted hexagonal crystals. The results are summarized in Fig. 5.

Each crystal morphology had its own specific fluorescence lifetime distribution, which was in all cases much faster than that of trimeric LHCII in detergent (4 ns, measured on the same set-up, using LHCII purified directly from spinach[35] or by solubilizing crystals[33]). The crystals all show a strong homogeneity of their fluorescence lifetimes. By contrast, fluorescence from regions in close vicinity to a crystal can be very different to that from the crystal itself, with fluorescence lifetimes ranging from 200 ps to 3.5 ns (*e.g.* pixels 4 and 5 in Fig. 3 and corresponding regions in Fig. 2 and 4). The fast (200 ps) decay was not observed in Fig. 2, due to the limited temporal resolution (200 ps per channel). Such regions have fluorescence spectra that are different to that of the crystal (Fig. 1 and ESI†). When a non-imaging technique is used, these spectroscopic features may be erroneously ascribed to the crystal itself. This shows the added value of SPIM and FLIM, as compared to non-imaging techniques, in studying the time-/spectrally-resolved fluorescence of LHCII crystals.

Discussion

LHCII plays an important role in light harvesting and photoprotection in photosynthesis, and can exist in different functional states (*e.g.* ref. 41). Whereas the research field has benefitted greatly from the crystal structures of LHCII,[33,34] (time-resolved) fluorescence has been used as a signature proxy for the functional state. It was shown that the fluorescence of the crystals is strongly quenched relative to that of LHCII trimers in detergent and it was concluded that each LHCII complex within the crystal had adopted a quenched state.[25] However, it was recently argued that at 100 K fluorescence quenching of LHCII crystals is only weak, and that it is not due to the fact that all LHCIIs are in a quenched state, but that it is caused by the presence of a (small) number of random quenchers that quench fluorescence of many, energetically coupled, nearby trimers.[23]

At room temperature, the fluorescence of crystals of different sizes, morphologies and ages is quenched in all cases (Fig. 2–5). Resonance Raman measurements on the crystals are consistent with this finding, indicating a conformation similar to quenched aggregated LHCII rather than to isolated trimers for all the crystals measured (see ESI†). The quenching observed here is stronger than that reported for similar crystals in our previous work.[25] The difference is mainly due to technical improvements since those first experiments: the background signal has decreased ~10-fold, and the instrument response function can be measured far more accurately.

A comparison with the more recent results of Barros *et al.*[24] is more difficult, because those measurements were performed at 100 K. They showed that the 100 K fluorescence emission spectra of LHCII crystals can be strongly distorted by

Table 1 Summary of the results depicted in Fig. 3 and 4: fluorescence lifetimes ($\langle\tau\rangle$ and τ_i, in ps), and relative amplitudes (p_i) in brackets, at different detection wavelengths (λ_{det})

	λ_{det}/nm	Rod	Big crystal	Region around pixel 4[a]	Region around pixel 5[a]
Mono-exponential fit					
τ_1	700[b]	510–520	530–570	650–900	1700–2300
	730[c]	440–470	480–520	540–630	1000–1400
Bi-exponential fit					
$\langle\tau\rangle$	700[b]	440–470	500–525	450–500	1200–2000
$\langle\tau\rangle$	730[c]	410–440	450–500	440–520	900–1200
$\tau_1(p_1)$	700[b]	330–400 (0.85–0.90)	380–480 (0.75–0.90)	230–350 (0.85–0.90)	370–550 (0.40–0.60)
$\tau_2(p_2)$	700[b]	750–1000 (0.10–0.15)	750–1000 (0.10–0.25)	1200–2100 (0.10–0.15)	2100–3500 (0.40–0.60)

[a] Pixels marked in Fig. 3. [b] Detection at 670–730 nm. [c] Detection at 710–750 nm.

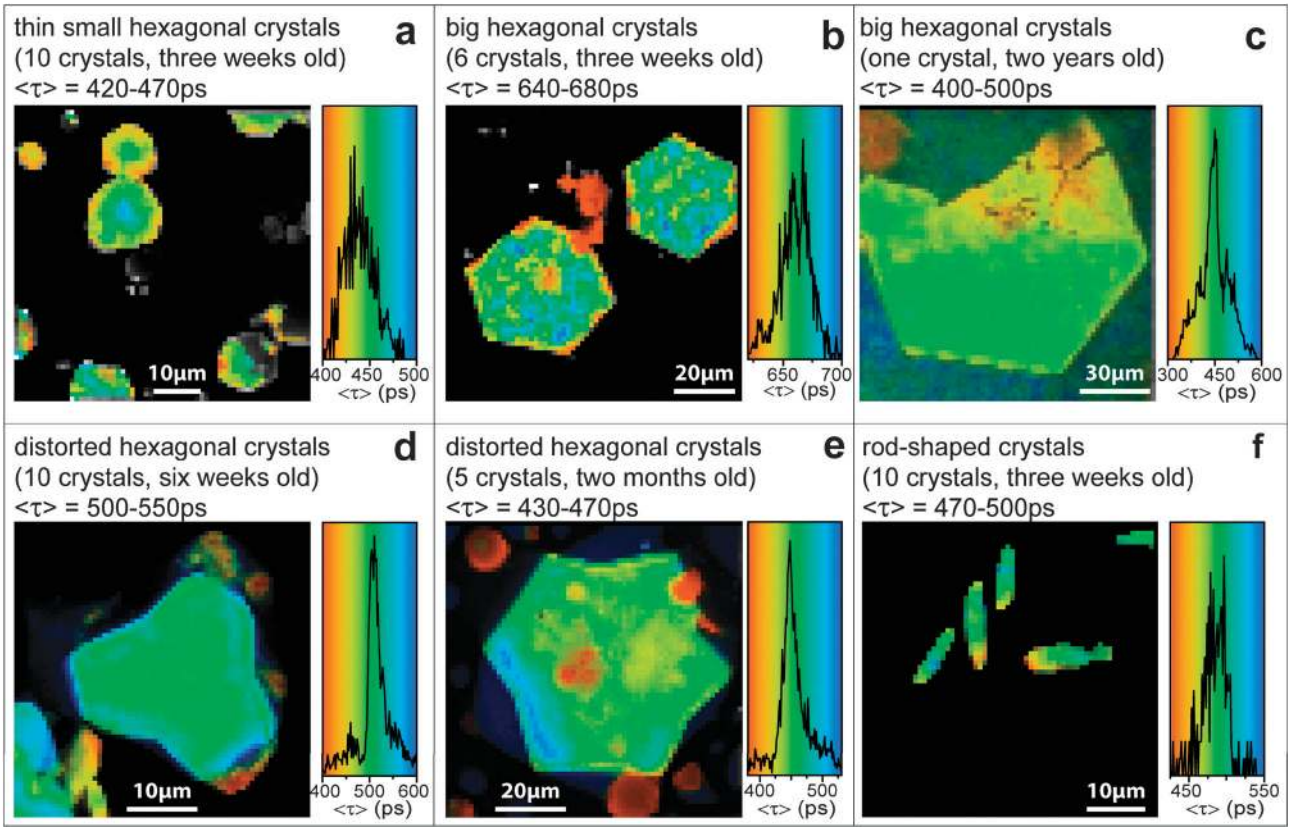

Fig. 5 Summary of results of time-resolved fluorescence of a large number of LHCII crystals. Each panel contains the results of one crystal type. Each contains a typical false-colour image of the average fluorescence lifetime ($\langle\tau\rangle$), and the corresponding $\langle\tau\rangle$-frequency histogram. Additionally, the $\langle\tau\rangle$-range of each crystal morphology is provided. This range is determined from the $\langle\tau\rangle$-frequency histogram of all pixels of the crystals of that particular crystal morphology, and corresponds to an interval (cantered around the median $\langle\tau\rangle$) that encompasses 95% of the pixels. Many 2 year old crystals are heavily damaged, so only one suited for FLIM (c).

reabsorption, which can explain some of the spectral features in ref. 25. Room temperature spectral imaging microscopy (SPIM) confirms the strong effect of reabsorption: the spectra show a strong red-shift upon increasing the excitation/detection depth relative to the crystal surface (Fig. 1). In FLIM we therefore worked selectively at the crystal surface.

The room temperature crystal spectra show characteristics of aggregation (in particular broadening). This indicates that for trimers in the crystal at room temperature, spectral changes occur (as compared to isolated trimers) that resemble those upon aggregation-induced quenching. The fluorescence intensity after correction for absorption of excitation light and reabsorption of emitted light is constant in the crystal, demonstrating that the fluorescence quenching is the same throughout the crystal (ESI†).

Barros *et al*. stated that at 100 K, LHCII crystals are only weakly quenched, as judged from the average fluorescence lifetime.[24] However, this conclusion depends on the used definition of average fluorescence lifetime ($\langle\tau\rangle$). The $\langle\tau\rangle$ of a fluorescence decay of N components can be calculated in different ways from the amplitudes p_i, fractions $f_i = p_i\tau_i$ and fluorescence lifetimes τ_i of the ith component of the fluorescence decay. The current work, and that of Pascal *et al*.[25] used the amplitude-weighted average lifetime $\langle\tau\rangle_{amp} = \sum_{i=1}^{N} p_i\tau_i \Big/ \sum_{i=1}^{N} p_i$, which is directly proportional to the fluorescence quantum yield (and inversely proportional to the extent of quenching).[39] Barros *et al*.[24] used the intensity-weighted average lifetime $\langle\tau\rangle_{int} = \sum_{i=1}^{N} f_i\tau_i \Big/ \sum_{i=1}^{N} f_i = \sum_{i=1}^{N} p_i\tau_i^2 \Big/ \sum_{i=1}^{N} p_i\tau_i$, which is not directly proportional to the fluorescence quantum yield, and the contribution of long-lived components is overestimated relative to that of the short-lived components.[39] When discussing the extent of fluorescence quenching, it is therefore appropriate to use $\langle\tau\rangle_{amp}$ and not $\langle\tau\rangle_{int}$. The difference between $\langle\tau\rangle_{amp}$ and $\langle\tau\rangle_{int}$ is illustrated in Table 2. For the data of Barros *et al*. the amplitude-weighted average lifetime (0.7 ns) is approximately 3 times shorter than the reported intensity-weighted average lifetime (2 ns) (based on ESI of ref. 24). So at 100 K the fluorescence of those crystals is quenched 7-fold relative to unquenched LHCII (which has a fluorescence lifetime of 5.1 ns at 100 K).[42] If the slowly decaying component (>1 ns) is

Table 2 Amplitude- and intensity-weighted average fluorescence lifetimes of the current work and ref. 24

	$\langle\tau\rangle_{amp}$/ns	$\langle\tau\rangle_{int}$/ns	$\langle\tau\rangle'_{amp}$/ns	$\langle\tau\rangle'_{int}$/ns
This work[a]	0.51	0.57	0.67[b]	1.4[b]
Ref. 24	0.70	2.0	0.45[c]	0.64[c]

[a] Averaged over the large crystal in Fig. 4. [b] Calculated with an additional 5% component of 3 ns. [c] Calculated without the 8% component of 3.8 ns.

ascribed to free LHCII and/or free pigments and therefore omitted from calculations, then $\langle\tau\rangle_{amp}$ would be 0.45 ns, and the quenching would be more than 10-fold (Table 2). This demonstrates that *all* crystal morphologies of plant LHCII studied up to now (including the one measured by Barros *et al.*) are in a quenched state. For comparison, Table 2 also shows $\langle\tau\rangle_{int}$ for the current data.

It is interesting to note that the fluorescence quenching at 100 K and at room temperature are similar. Upon lowering the temperature the intra-trimeric energy transfer slows down.[43] In a crystal lattice of energetically coupled LHCII trimers this will reduce the distance over which excitons can migrate.[28,44] If random quenchers are present in the crystal, then their quenching efficiency is expected to decrease with decreasing exciton migration. As a consequence the fluorescence quenching should decrease at 100 K relative to that at room temperature. Such an increase of fluorescence is, however, not observed, suggesting that excitons do not have to travel far to reach the quenching site. This is consistent with intratrimeric quenching, but also with a high concentration of random quenchers.

The concentration, nature and quenching strength of random quenchers are expected to vary within and between crystals, and as a consequence to lead to a distribution/variation of lifetimes (within and between crystals). This is not observed: the variation of fluorescence lifetimes within single crystals is small (typically 20–50 ps, see Table 1 and Fig. 4 and 5). However, the excited volume of the crystal contains on the order of 10^5 LHCII trimers. Therefore local variations of fluorescence lifetimes on a smaller scale cannot be directly visualized, but they may show up as multi-exponentiality of the decay kinetics. However, the fluorescence decay of the different crystals is nearly mono-exponential, which is very different from the results on LHCII aggregates.[36,45] Moreover, different crystals with similar morphology have very similar lifetimes whereas crystals with different morphologies also have different fluorescence lifetimes (Fig. 5), even if they have been formed in the same crystallization drop (Fig. 2). The difference in fluorescence lifetime for different crystal morphologies is much larger than the variation of fluorescence lifetimes within and among crystals of the same morphology. Interestingly, the oldest (partly-damaged) crystal is also the most quenched (Fig. 5). The damaged part of the crystal is strongly quenched and has a broad distribution of lifetimes ($\sim$330–420 ps), as expected for random quenchers, thus confirming the quenching mechanism proposed by Barros *et al.*[24] However, the undamaged part of the crystal has a narrower distribution of fluorescence lifetimes (430–480 ps), and yet it is also strongly quenched. This indicates that both "random quenchers" and "intratrimeric quenching" can occur in LHCII crystals, but that "random quenchers" are mainly present in damaged crystals.

Very small structural variations can have large excited-state spectral and kinetic effects: *e.g.* a 0.006% volume change can lead to strong fluorescence quenching,[27] and theoretical studies suggest spectral differences[26] between the two highly similar crystal structures.[33,34] The overall conclusion must be that, while wholesale structural changes at the protein level are not involved, relatively minor movements of certain key pigments result in dramatic changes at the level of function.

In fact, there are several indications that conformational switching and concomitant fluorescence changes take place in LHCII, *e.g.* with LHCII in liposomes and micelles,[30] under high hydrostatic pressure,[27] with LHCII in polyacrylamide gels,[29] and in single LHCII trimers.[41] In the latter two experiments strong quenching occurs in the absence of aggregation, and hence without feasible strong quenching by impurities, indicating that changes *within* the LHCII complex are responsible for quenching. The quenching in gels is accompanied by spectral changes (fluorescence/absorption/circular dichroism) similar to those observed upon aggregation, which indicates that similar changes *within* LHCII take place upon quenching with or without aggregation. Also, differences between linear and circular dichroism of LHCII trimers, lamellar aggregates and unstacked thylakoid membranes show variability between LHCII pigment interactions, which must be due to (small) structural changes.[46]

Conclusions

From the present study of time-resolved fluorescence of LHCII crystals we conclude that:

- the fluorescence is strongly quenched ($\sim$8$\times$ relative to trimeric LHCII in detergent) in all types of LHCII crystals studied, which indicates that the fluorescence quenching is an intrinsic property of the LHCII complexes in the crystal, and is not due to crystal impurities;
- the fluorescence decay is nearly mono-exponential and very homogeneous throughout the crystal, again pointing to fluorescence quenching as an intrinsic property of LHCII (volume changes as small as 0.006% can induce strong quenching in LHCII,[27] and aggregation leads to very multi-exponential fluorescence decay behavior (*e.g.* ref. 36 and 45));
- different crystal morphologies correspond to different fluorescence lifetimes, even for crystals being formed within the same crystallization drop, strongly suggesting that (very) small structural differences between trimers in the different crystals can lead to small lifetime differences.

Acknowledgements

We are grateful to Dr Chao Wang and Xiaowei Pan from the National Laboratory of Biomacromolecules, Institute of Biophysics, Beijing, for their assistance in preparing LHCII crystals and to Prof. Wenrui Chang for giving us two-years old LHCII crystals prepared in that laboratory.

B. van Oort is supported by a Rubicon Grant of the Netherlands Organisation for Scientific Research.

Notes and references

1 V. I. Novoderezhkin, M. A. Palacios, H. van Amerongen and R. van Grondelle, *J. Phys. Chem. B*, 2004, **108**, 10363–10375.
2 V. I. Novoderezhkin and R. van Grondelle, *Phys. Chem. Chem. Phys.*, 2010, **12**, 7352–7365.
3 R. Croce and H. van Amerongen, *J. Photochem. Photobiol., B*, 2011, DOI: 10.1016/j.jphotobiol.2011.02.015.
4 P. Horton, A. V. Ruban and R. G. Walters, *Annu. Rev. Plant Physiol. Plant Mol. Biol.*, 1996, **47**, 655–684.
5 S. de Bianchi, M. Ballottari, L. Dall'Osto and R. Bassi, *Biochem. Soc. Trans.*, 2010, **38**, 651–660.

6 P. Horton and A. V. Ruban, *J. Exp. Bot.*, 2005, **56**, 365–373.
7 K. K. Niyogi, X.-P. Li, V. Rosenberg and H.-S. Jung, *J. Exp. Bot.*, 2005, **56**, 375–382.
8 B. Demmig-Adams, *Biochim. Biophys. Acta*, 1990, **1020**, 1–24.
9 X. P. Li, O. Bjorkman, C. Shih, A. R. Grossman, M. Rosenquist, S. Jansson and K. K. Niyogi, *Nature*, 2000, **403**, 391–395.
10 P. Horton, A. V. Ruban, D. Rees, A. A. Pascal, G. Noctor and A. J. Young, *FEBS Lett.*, 1991, **292**, 1.
11 A. R. Holzwarth, Y. Miloslavina, M. Nilkens and P. Jahns, *Chem. Phys. Lett.*, 2009, **483**, 262–267.
12 T. J. Avenson, T. K. Ahn, D. Zigmantas, K. K. Niyogi, Z. Li, M. Ballottari, R. Bassi and G. R. Fleming, *J. Biol. Chem.*, 2008, **283**, 3550–3558.
13 T. K. Ahn, T. J. Avenson, M. Ballottari, Y.-C. Cheng, K. K. Niyogi, R. Bassi and G. R. Fleming, *Science*, 2008, **320**, 794–797.
14 M. Mozzo, F. Passarini, R. Bassi, H. van Amerongen and R. Croce, *Biochim. Biophys. Acta*, 2008, **1777**, 1263–1267.
15 A. R. Crofts and C. T. Yerkes, *FEBS Lett.*, 1994, **352**, 265–270.
16 M. G. Müller, P. Lambrev, M. Reus, E. Wientjes, R. Croce and A. R. Holzwarth, *ChemPhysChem*, 2010, **11**, 1289–1296.
17 N. E. Holt, D. Zigmantas, L. Valkunas, X.-P. Li, K. K. Niyogi and G. R. Fleming, *Science*, 2005, **307**, 433–436.
18 H. van Amerongen and R. van Grondelle, *J. Phys. Chem. B*, 2001, **105**, 604–617.
19 S. S. Lampoura, V. Barzda, G. M. Owen, A. J. Hoff and H. van Amerongen, *Biochemistry*, 2002, **41**, 9139–9144.
20 S. Bode, C. C. Quentmeier, P. N. Liao, N. Hafi, T. Barros, L. Wilk, F. Bittner and P. J. Walla, *Proc. Natl. Acad. Sci. U. S. A.*, 2009, **106**, 12311–12316.
21 A. V. Ruban, A. J. Young and P. Horton, *Biochemistry*, 1996, **35**, 674–678.
22 A. V. Ruban, R. Berera, C. Ilioaia, I. H. M. van Stokkum, J. T. M. Kennis, A. A. Pascal, H. van Amerongen, B. Robert, P. Horton and R. van Grondelle, *Nature*, 2007, **450**, 575–579.
23 H. A. Frank, A. Cua, V. Chynwat, A. Young, D. Gosztola and M. R. Wasielewski, *Photosynth. Res.*, 1994, **41**, 389.
24 T. Barros, A. Royant, J. Standfuss, A. Dreuw and W. Kuhlbrandt, *EMBO J.*, 2009, **28**, 298–306.
25 A. A. Pascal, Z. F. Liu, K. Broess, B. van Oort, H. van Amerongen, C. Wang, P. Horton, B. Robert, W. R. Chang and A. Ruban, *Nature*, 2005, **436**, 134–137.
26 F. Müh, M. E.-A. Madjet and T. Renger, *J. Phys. Chem. B*, 2010, **114**, 13517–13535.
27 B. van Oort, A. van Hoek, A. V. Ruban and H. van Amerongen, *J. Phys. Chem. B*, 2007, **111**, 7631–7637.
28 A. V. Ruban, J. P. Dekker, P. Horton and R. van Grondelle, *Photochem. Photobiol.*, 1995, **61**, 216–221.
29 C. Ilioaia, M. P. Johnson, P. Horton and A. V. Ruban, *J. Biol. Chem.*, 2008, **283**, 29505–29512.
30 I. Moya, M. Silvestri, O. Vallon, G. Cinque and R. Bassi, *Biochemistry*, 2001, **40**, 12552–12561.
31 A. M. Gilmore, T. L. Hazlett and Govindjee, *Proc. Natl. Acad. Sci. U. S. A.*, 1995, **92**, 2273–2277.
32 L. Dall'Osto, S. Cazzaniga, H. North, A. Marion-Poll and R. Bassi, *Plant Cell*, 2007, **19**, 1048–1064.
33 Z. F. Liu, H. Yan, K. Wang, T. Kuang, J. Zhang, L. Gui and W. Chang, *Nature*, 2004, **428**, 287–292.
34 J. Standfuss, A. C. Terwisscha van Scheltinga, M. Lamborghini and W. Kühlbrandt, *EMBO J.*, 2005, **24**, 919–928.
35 A. V. Ruban, P. J. Lee, M. Wentworth, A. J. Young and P. Horton, *J. Biol. Chem.*, 1999, **274**, 10458–10465.
36 B. van Oort, A. van Hoek, A. V. Ruban and H. van Amerongen, *FEBS Lett.*, 2007, **581**, 3528–3532.
37 B. van Oort, A. Amunts, J. W. Borst, A. van Hoek, N. Nelson, H. van Amerongen and R. Croce, *Biophys. J.*, 2008, **95**, 5851–5861.
38 A. Pascal, U. Wacker, K.-D. Irrgang, P. Horton, G. Renger and B. Robert, *J. Biol. Chem.*, 2000, **275**, 22031–22036.
39 J. R. Lakowicz, *Principles of Fluorescence Spectroscopy*, Kluwer Academic/Plenum Publishers, New York, 3rd edn, 2006, vol. 1, pp. 97–155.
40 M. L. Johnson and L. M. Faunt, in *Methods in Enzymology*, ed. L. Brand and M. L. Johnson, Academic Press, San Diego, 1992, vol. 210, pp. 1–37.
41 T. P. J. Kruger, V. I. Novoderezhkin, C. Ilioaia and R. van Grondelle, *Biophys. J.*, 2010, **98**, 3093–3101.
42 M. A. Palacios, F. L. de Weerd, J. A. Ihalainen, R. van Grondelle and H. van Amerongen, *J. Phys. Chem. B*, 2002, **106**, 5782–5787.
43 S. Savikhin, H. van Amerongen, S. L. Kwa, R. van Grondelle and W. S. Struve, *Biophys. J.*, 1994, **66**, 1597–1603.
44 H. van Amerongen, L. Valkunas and R. van Grondelle, *Photosynthetic excitons*, World Scientific Publishing, Singapore, 2000.
45 V. Barzda, C. J. de Grauw, J. Vroom, F. J. Kleima, R. van Grondelle, H. van Amerongen and H. C. Gerritsen, *Biophys. J.*, 2001, **81**, 538–546.
46 P. H. Lambrev, Z. Varkonyi, S. Krumova, L. Kovacs, Y. Miloslavina, A. R. Holzwarth and G. Garab, *Biochim. Biophys. Acta*, 2007, **1767**, 847–853.

Electronic Supplementary Material (ESI) for Physical Chemistry Chemical Physics

Supplementary material

Modelling of reabsorption effects

The intensity and spectrum of the fluorescence detected in SPIM depends on several factors:

1. the photon density at the confocal excitation spot.
2. the fluorescence spectrum and quantum yield of the emitting species at the confocal excitation spot
3. the re-absorption of emitted photons by the sample
4. the detection efficiency, which is not expected to vary for detection in different positions in the crystal.

Factors 1 and 4 are both affected by the absorption spectrum of the medium between the microscope objective and the location confocal spot. For a confocal spot at increasing depth in an LHCII crystal, the excitation and detection light travel through an increasingly thick section of LHCII, leading to increased (re-)absorption. This leads to decreased total detected fluorescence, and a red-shift of the fluorescence, because the high-energy (blue) emission photons have a higher probability of being absorbed than red emission photons.

We modelled the spectral dependence on vertical excitation/detection position, by multiplication of the emission spectrum with the transmission spectrum ($T=10^{-\varepsilon(\lambda)cz}$) for a path length of z through the crystal, where c is the concentration of trimeric LHCII in the crystal (2.5 mM[1]) and $\varepsilon(\lambda)$ the wavelength dependent molecular extinction coefficient of the trimeric LHCII. The calculations were done for emission spectra of either trimeric LHCII, aggregates of trimeric LHCII or the spectrum detected by SPIM on the outer edge of the crystal. These all gave very similar results.

Light travelling to and from the focal spot of the objective experiences different path lengths (with different extents of (re-)absorption), due to the high numerical aperture of the objective (1.4). With this numerical aperture the angle under which light travels to/from the focal spot ranges from 0 to ~69°. Different angles contribute to different extents to the total light travelling to/from the focal spot, which was taken into account in the modelling. The final result was convolved with the vertical point spread function.

The modelled spectra are very similar to the experimental spectra (Figure S1). The differences are well within the experimental/modelling uncertainties. The main uncertainties in modelling arise from the unknown refractive index inside the crystal, the uncertainty in the red tail of the absorption spectrum and of the absorption at the excitation wavelength (543 nm), the effect of internal scattering and the uncertainty in the point spread function. From the results in Figure S1, we conclude that within the current precision, the observed spectral dependence on vertical position in the crystal can be completely attributed to (re-)absorption effects. Thus, there are no indications that the fluorescence intensity and spectrum vary vertically in the crystal. This conclusion also holds for excitation at 488 nm and 633 nm, where the main difference is in the lower penetration depth of the excitation light into the crystal.

The spectrum of each voxel of a SPIM dataset was subjected to cubic interpolation. The positions of the maxima of these interpolated spectra are plotted in false-colour in Figure S2, for different horizontal cross-sections of they crystal. There are no indications that the fluorescence intensity and spectrum varies horizontally in the crystal.

From the results in Figures S1 and S2 it can therefore be concluded that the fluorescence spectrum and quantum yield do not vary throughout the crystal. It should be noted that variations smaller that the microscope's psf would be hard to detect.

The total fluorescence of each pixel of data in Fig. S2 was used for a 3D reconstruction (Fig. S3). The crystal has a distinct shape, with tilted surfaces.

The Raman spectra of several crystals were measured in the chlorophyll *b* carbonyl and neoxanthin ν_4 regions. All spectra showed the same characteristic difference with LHCII in detergent buffer. The spectrum of a typical crystal is shown in Figure S4. Most samples also showed strong contributions of free LHCII and/or free pigments present in the crystallization buffer. This presence was also evident from the fluorescence microscopy data (see main text), but there its contribution was readily eliminated by focussing on the crystallized regions only. The contribution of free LHCII/pigments precludes quantitative comparison of the Raman spectra of the different crystal types.

Reference

1 Z. F. Liu, H. Yan, K. Wang, T. Kuang, J. Zhang, L. Gui and W. Chang, *Nature*, 2004, **428**, 287-292.

Supplementary Figures

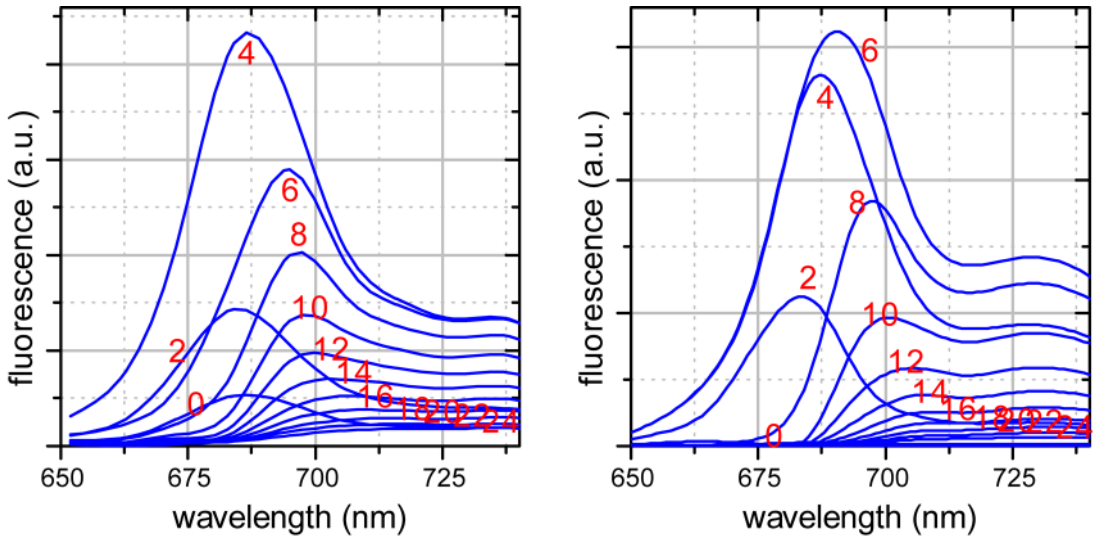

Figure S1 Fluorescence emission spectra detected at different vertical positions in an LHCII crystal (left), and modelled spectra. Vertical positions (in μm) are indicated in red.

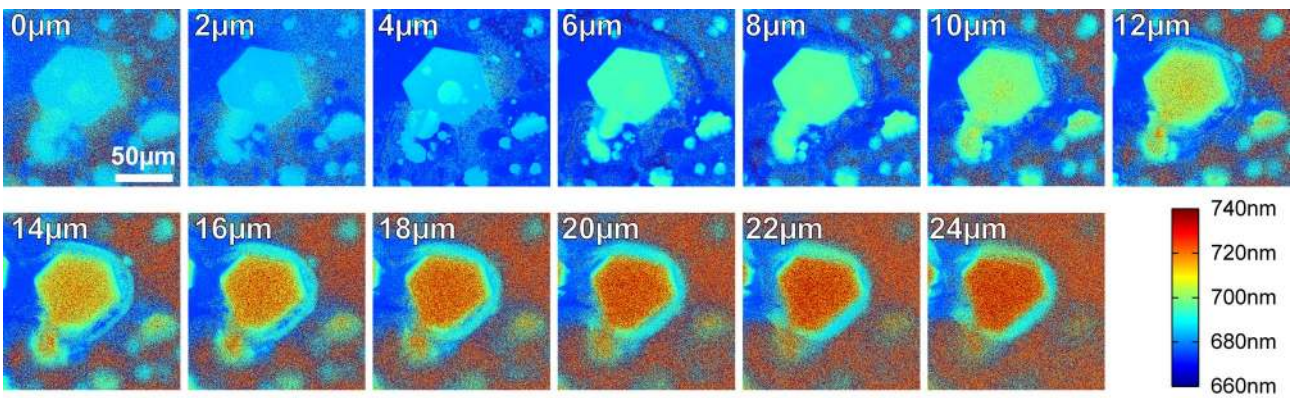

Figure S2 SPIM results of a five-week-old LHCII crystal. False-colour images of the wavelength of maximal emission at different horizontal cross-sections of the crystal. The relative vertical position is indicated in the upper left corner.

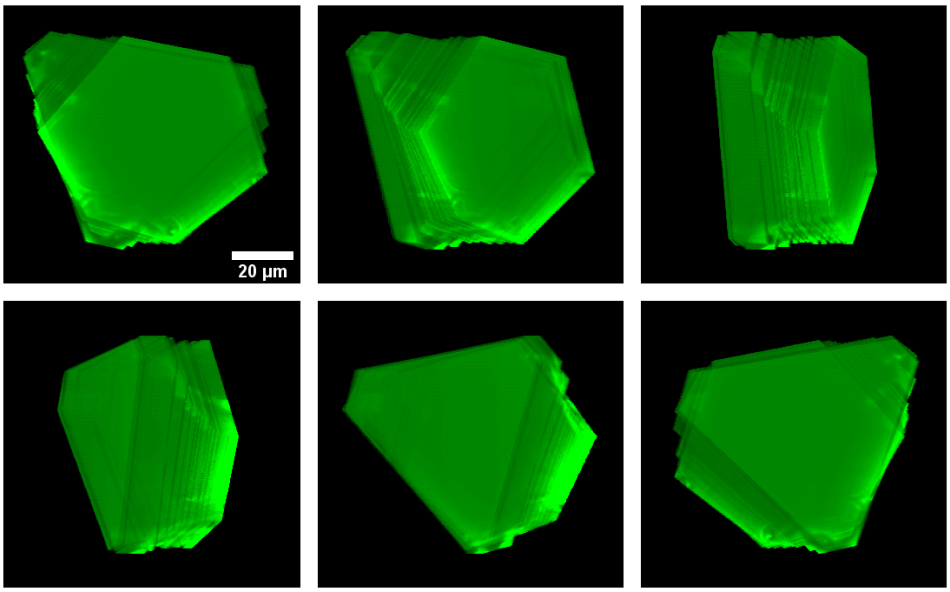

Figure S3 Results of SPIM measurements of one LHCII crystal. Five projections of a 3D reconstruction based on 3D imaging of total chlorophyll fluorescence of the LHCII crystal in Figs. 1 and S1.

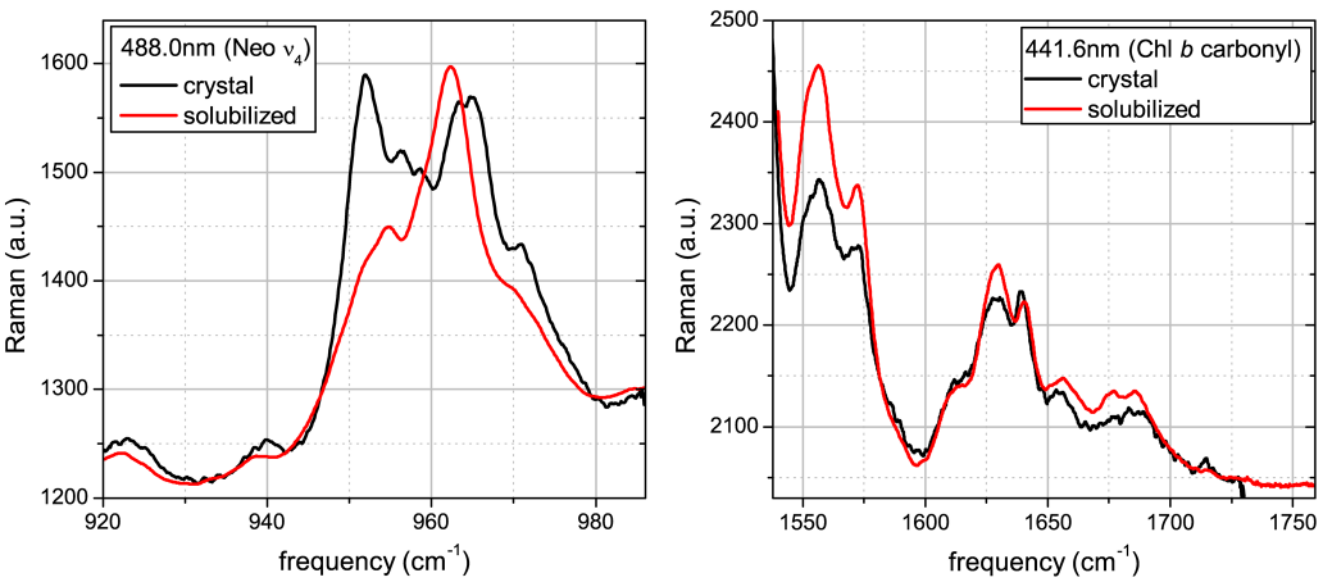

Figure S4 77K Raman spectra of a single LHCII crystal, in the spectral regions of neoxanthin ν_4 (left, excitation at 488.0nm) and Chl *b* carbonyl (right, excitation at 441.6nm).